Integral-Equation Study of Ray Effects and Natural-Mode Resonances in a 2-D Dielectric Prism

Ilya O. Sukharevsky[1,2], Ayhan Altintas[3]

[1] Communication and Spectrum Management Research Center, Bilkent University, Ankara, Turkey, i.sukharevsky@gmail.com
[2] Laboratory of Micro and Nano Optics, Institute of Radio-Physics and Electronics NASU, Ukraine
[3] Faculty of Engineering and Natural Sciences, Abdullah Gul University, Kayseri, Turkey, altintas@ee.bilkent.edu.tr

***Abstract*— We analyze the interplay of two different types of electromagnetic behavior demonstrated by a 2-D dielectric prism: Geometrical Optics and resonance. As it is shown, the first is responsible, for instance, for enhanced reflection from an isosceles 90-degree prism of arbitrary epsilon and size, if illuminated from the base. The second is responsible for the peaks in the total scattering and absorption cross-sections (RCS) at the natural-mode frequencies. The numerical model is based on Nystrom discretization of Muller-type integral equations that provides guarantied convergence.**

***Index Terms*—dielectric cylinder, boundary integral equations, radar cross-section, natural-mode resonances.**

I. INTRODUCTION

In spite of its simple shape, a triangular dielectric cylinder has not been studied sufficiently in terms of the scattering characteristics in the wide range of frequencies and for varying parameters (as an apex angle, for example). Some partial studies around this topic have performed by asymptotic methods [1], or by solving elementary integral equations (IEs) [2] that do not provide trusted results, since they are contaminated with spurious eigenvalues.

In the scattering of waves by 2-D homogeneous dielectric bodies, boundary IE techniques are one of the most popular computational tools. Still amazingly many researchers use the forms of such IE that are not fully equivalent to the original boundary-value problem, because of the presence of infinite set of spurious real-valued eigenvalues [3-4]. This pitfall can be avoided by using the Muller boundary IE (MBIE) that is a pair of coupled second-kind IE for the field tangential components [5-7].

In this paper, we use MBIE to analyze accurately the interplay of the ray-effects and the internal resonances in the scattering of waves by a triangular prism with rounded edges. The numerical algorithm used has been validated in our previous work [8]. We demonstrate that practically important characteristics such as total scattering cross-section (TSCS) and radar cross-section (RCS) can be manipulated on wide scale by varying the shape of the triangle.

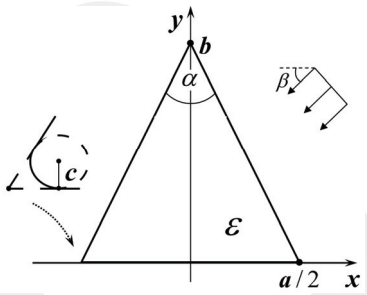

Fig. 1. Cross-section of a 2D isosceles prism of the relative dielectric permittivity ε, the base a, and the height b, with rounded edges, illuminated by a plane wave incident under the angle β.

II. PROBLEM FORMULATION

A. Formulation and Muller Equations

Consider an electromagnetic plane wave incident at the angle β on a dielectric cylinder of triangular cross-section (a prism) as depicted in Fig. 1. The prism has relative dielectric permittivity ε, base d, height h, and cross-section contour L. The host medium is free space.

Then the incident plane-wave z-component of the E (H) field in the case of the E (H) polarization is given as $U^{inc}(\vec{r}) = e^{-ik_0(x\cos\beta + y\sin\beta)}$, where $\vec{r} = (x, y)$, $k_0 = \omega / c$, and c is the free-space light velocity. In the presence of prism, the total field is $U(\vec{r}) = U^{inc} + U^{sc}$. Then $U^{sc}(\vec{r})$ must satisfy relevant Helmholtz equations inside and outside the prism and provide the continuity of the tangential components across L. For the uniqueness of the solution, it must also satisfy Sommerfeld radiation condition and condition of local energy finiteness.

Derivation of MBIE uses the Green's formulas and can be found in [6], so that we present only the resulting equations,

$$U(\vec{r}) + \int_L K_{11}(\vec{r}, \vec{r}\,')U(\vec{r}\,')d\vec{r}\,' - \int_L K_{12}(\vec{r}, \vec{r}\,')V(\vec{r}\,')d\vec{r}\,' = U^{inc}(\vec{r}), \quad (1)$$

$$\frac{1+p}{2}V(\vec{r}) + \int_L K_{21}(\vec{r}, \vec{r}\,')U(\vec{r}\,')d\vec{r}\,' - \int_L K_{22}V(\vec{r}\,')d\vec{r}\,' = V^{inc}(\vec{r}), \ \vec{r} \in L \quad (2)$$

Here, $V(\vec{r}) = \partial U(\vec{r})/\partial n$ is the limit value of the normal derivative of the total field on the closed contour L of the prism from the inner side of it, the normal unit vector $\vec{n}$ is directed to the outer domain D_e (free space), $d\vec{r}\,'$ is the elementary arc length, and the constant is $p = 1$ in the E-polarization case and $p = 1/\varepsilon$ in the H-polarization case.

The kernels of MBIE have the following form (see [5,6]):

$$K_{11} = \frac{\partial G_i}{\partial n'} - \frac{\partial G_e}{\partial n'}, \quad K_{12} = G_i - pG_e, \tag{3}$$

$$K_{21} = \frac{\partial^2 G_i}{\partial n\,\partial n'} - \frac{\partial^2 G_e}{\partial n\,\partial n'}, \quad K_{22} = \frac{\partial G_i}{\partial n} - p\frac{\partial G_e}{\partial n} \tag{4}$$

where $G_{(i,e)} = G_{(i,e)}(\vec{r},\vec{r}\,') = (i/4)H_0^{(1)}(k_{i,e}\rho)$ are the Green's functions of the corresponding homogeneous media, $k_e = k_0$, $k_i = k_0\sqrt{\varepsilon}$, and $\rho = |\vec{r} - \vec{r}\,'|$.

B. Discretization and Numerical Algorithm

If L is a Lyapunov surface, then the kernel functions have at most weak logarithmic singularities (see [6]), and then (1), and (2) are a Fredholm second kind IE. This guarantees the convergence of usual schemes of its discretization. However, the assumption of L to be a Lyapunov surface is essential here, since (1), (2) are derived by using theorems of classical potential theory [10], and in non-regular points of contour the unit normal vector and some field components and their derivatives are not defined. In order to overcome this problem, we can approximate irregular curve by a smooth one and then apply quadratures for the 2π-periodic functions [6]. For example, this can be done using the trigonometric polynomial approximation (truncated Fourier series). However Fourier series are known to diverge for the polygonal contours.

Therefore, as shown in Fig. 1, we subdivide the strip contour L into separate smooth segments that is four straight intervals, extract logarithmic singularities from (3) and (4), and apply quadratures on each segment. The discretization performed in this manner is not sensitive to the irregularities of the contour so far as the interpolation nodes do not coincide with edge points. Full analysis of the kernels at $\vec{r} \to \vec{r}\,'$ can be found in [6], [7]. Denoting the contour curvature $\varsigma(\vec{r})$, we introduce new continuous kernels as follows:

$$\tilde{K}_{11} = \begin{cases} K_{11} = \dfrac{i}{4}\left[-k_i H_1^{(1)}(k_i\rho) + k_e H_1^{(1)}(k_e\rho)\right]\dfrac{\partial\rho}{\partial n'}, & \vec{r} \neq \vec{r}\,' \\ 0, & \vec{r} = \vec{r}\,' \end{cases} \tag{5}$$

$$\tilde{K}_{12} = \begin{cases} K_{12} = \dfrac{i}{4}\left[H_0^{(1)}(k_i\rho) - pH_0^{(1)}(k_e\rho)\right], & \vec{r} \neq \vec{r}\,' \\ (1-p)\left(\dfrac{i}{4} - \dfrac{C}{2\pi}\right) - \dfrac{1}{2\pi}\left(\ln\dfrac{k_i}{2} - p\ln\dfrac{k_e}{2}\right), & \vec{r} = \vec{r}\,' \end{cases} \tag{6}$$

$$\tilde{K}_{22} = \begin{cases} K_{22} = \dfrac{i}{4}\left[pk_e H_0^{(1)}(k_e\rho) - k_i H_0^{(1)}(k_i\rho)\right]\dfrac{\partial\rho}{\partial n'}, & \vec{r} \neq \vec{r}\,' \\ \dfrac{1-p}{4\pi}\varsigma(\vec{r}), & \vec{r} = \vec{r}\,' \end{cases} \tag{7}$$

$$\tilde{K}_{21} = \begin{cases} K_{21} = \dfrac{i}{8}\left[k_e^2 H_0^{(1)}(k_e\rho) - k_i^2 H_0^{(1)}(k_i\rho)\right. \\ \left. + k_i^2 H_2^{(1)}(k_i\rho) - k_e^2 H_2^{(1)}(k_e\rho)\right]\dfrac{\partial\rho}{\partial n}\dfrac{\partial\rho}{\partial n'} \\ + \dfrac{i}{4}\left[k_e^2 H_1^{(1)}(k_e\rho) - k_i^2 H_1^{(1)}(k_i\rho)\right]\dfrac{\partial^2\rho}{\partial n\,\partial n'}, & \vec{r} \neq \vec{r}\,' \\ \dfrac{k_i^2 - k_e^2}{4\pi}\left(\dfrac{i}{2} - C - \ln\dfrac{k_i}{2}\right) - \dfrac{1}{4\pi}\left(k_i^2\ln\dfrac{k_i}{2} - k_e^2\ln\dfrac{k_e}{2}\right), & \vec{r} = \vec{r}\,' \end{cases} \tag{8}$$

Introduce N sub-sections of the lengths Δ_j $(j = 1,...,N)$ of the segments of L and assume that unknown functions are constants at each sub-section. Then, after applying the rectangle rule for numerical integration, we obtain a matrix equation with respect to the unknowns,

$$U(\vec{r}_i) + \sum_{j=1}^{N}\tilde{K}_{11}(\vec{r}_i,\vec{r}_j)U(\vec{r}_j)\,|\,\Delta_j\,| - \sum_{j=1}^{N}\tilde{K}_{12}(\vec{r}_i,\vec{r}_j)V(\vec{r}_j)\,|\,\Delta_j\,| - (p-1)V(\vec{r}_i)\int_{\Delta_i}\ln\rho\,ds' = U^{inc}(\vec{r}_i), \tag{9}$$

$$(1/2)(1+p)V(\vec{r}_i) + \sum_{i=1}^{N}\tilde{K}_{21}(\vec{r}_i,\vec{r}_j)U(\vec{r}_j)\,|\,\Delta_j\,| - \sum_{i=1}^{N}\tilde{K}_{22}(\vec{r}_i,\vec{r}_j)V(\vec{r}_j)\,|\,\Delta_j\,| + \frac{k_i^2 - k_e^2}{4\pi}U(\vec{r}_i)\int_{\Delta_i}\ln\rho\,ds' = V^{inc}(\vec{r}_i), \tag{10}$$

As $\rho = |\vec{r} - \vec{r}\,'|$, the value of $\int_{L_i}\ln\rho\,ds'$ can be integrated analytically.

In computations, we have taken N = 600 in the case of a half-wavelength dielectric strip with $\varepsilon = 4$, and 200 to 1000 in the case of silver strip of $d = 150$ to 900 nm. This guaranteed the accuracy, in the far field, of the order of 10^{-4} and 10^{-3}, respectively (see Appendix II). Larger N for a metal strip are explained by the larger values of $|\varepsilon|$.

After finding the longitudinal component of the field scattered by the 2-D prism, $U^{sc}(x,y)$, and its derivative, we can calculate the values of RCS, TSCS and ACS that

$$\sigma_b = (4k_0)^{-1}\,|\,\Phi(\beta)\,|^2, \tag{11}$$

$$\sigma_{sc} = (8\pi k_0)^{-1}\int_0^{2\pi}|\,\Phi(\varphi)\,|^2 d\varphi\,. \tag{12}$$

Here, the far-field scattering pattern is

$$\Phi(\varphi) = \int_L e^{-ik_0(\vec{r}_0\cdot\vec{x})}\left[ik_0(\vec{n}\cdot\vec{r}_0)U + p\frac{\partial U}{\partial n}\right]ds, \tag{13}$$

U and $\partial U/\partial n$ are the limiting values of the inner field and its normal derivative on the boundary and $\vec{r}_0 = (\cos\varphi, \sin\varphi)$.

III. Numerical Results

A. GO Effects and Resonances of Isosceles 90-deg Triangle

A right-angle dielectric prism (apex angle α = 90°) shows

an interesting GO effect provided that the plane wave is incident from the half-space to which the flat base is looking at. Such a scatterer behaves similarly to a 90° corner reflector [9] – see the RCS dependence on β and a sketch in Fig. 10 of [1]. In the GO approximation, every ray impinging on the flat base experiences two refractions in accordance with Snell's law and two internal reflections and gets out of the prism in the backward direction. As we showed, the peak values of RCS at the normal on-base incidence are some five to ten times larger than for the apex angles α other than 90°. RCS dependences of the frequency are modulated with peaks, which betray the presence of internal resonances.

However, monostatic RCS is not the best tool for observation of the internal resonances on a dielectric scatterer because it characterizes only the far field and, more specifically, the field scattered in one (backward) direction. Better chances to detect them are provided by plotting the frequency dependences of TSCS, which is proportional to the total power taken by the scattered field to infinity in all directions.

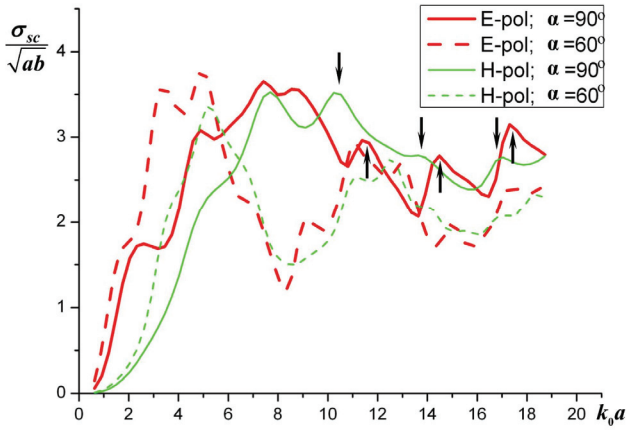

Fig. 2. Normalized TSCS of a triangular dielectric cylinder with $\varepsilon = 4$ as a function of the normalized frequency k_0a for two alternative polarizations at $\beta = 90°$ or 270° and two values of the apex angle, α =60° and 90°.

The plots in Fig. 2 show the frequency scans of the TSCS. Here, one should remember that, in the lossless case, the plots for β = 90° and 270° are identical due to the reciprocity theorem. The natural-mode resonances are visible as peaks of increased TSCS due to the underlying complex poles of the field as a function of frequency. They are broad because their Q-factors are rather low.

The resonances in rectangular prism are best excited if it is illuminated normally to the base, in either polarization. The corresponding in-resonance near field amplitude patterns are presented in Fig. 3 for three resonances indicated by arrows in Fig. 2. They demonstrate that adjacent resonances have the number of field variation along the sides of triangle that differ by one from each other.

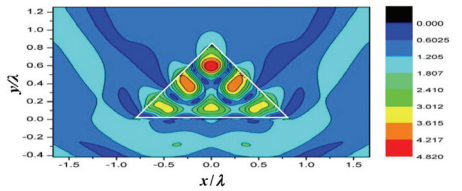

(a) $k_0a = 10.5$

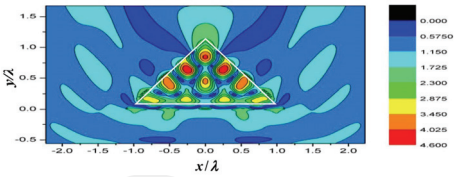

(b) $k_0a = 14$

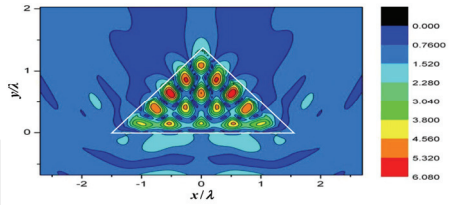

(c) $k_0a = 17$

Fig. 3. The near field and the normalized scattered far-field patterns of a triangular cylinder: $\alpha = 90^o$, $\varepsilon = 4$ and $\beta = 270^o$, H-wave excitation

B. *Resonances of a Regular Triangle*

In Fig. 4, we present the reliefs of RCS of an equilateral dielectric prism (here L is regular triangle). They visualize the frequencies of the internal resonances and show that they are best excited at the on-apex and on-facet incidence, with reduced RCS otherwise. This is explained by the properties of the modal field: it has three most prominent lobes of radiation along each of its apexes and three smaller lobes normally to each side. Note that the maxima in RCS become larger at higher frequencies or for larger prisms. This is a consequence of the fact that the associated natural modes have Q-factors growing up with the normalized frequency.

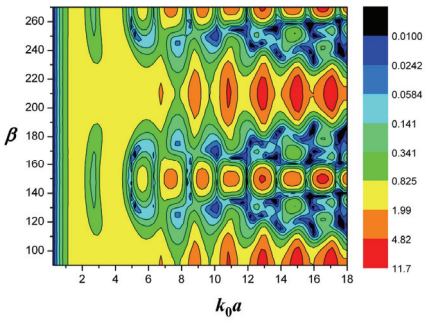

Fig. 4. Reliefs of the normalized RCS of a regular triangle prism ($\alpha = 90^o$) with $\varepsilon = 4$ as a function of the normalized frequency k_0a and the angle of incidence β, in the E-polariztion case.

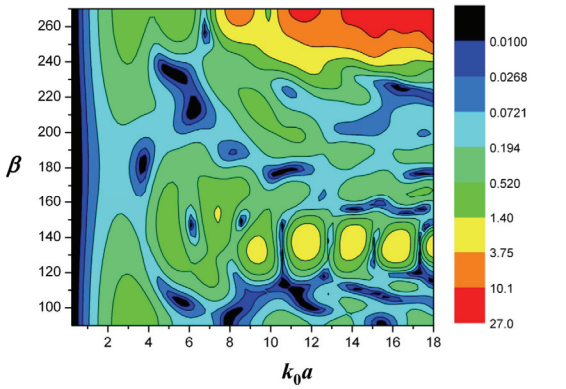

(a)

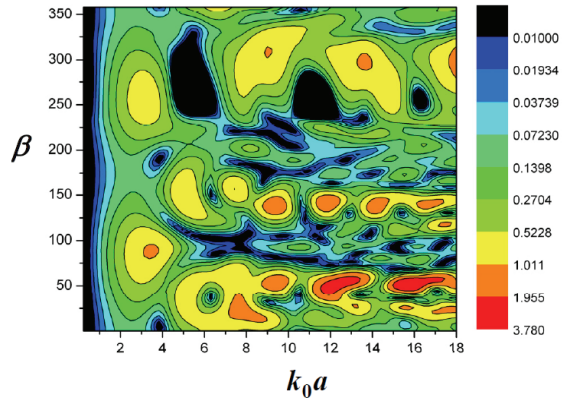

(b)

Fig. 5. Reliefs of the normalized RCS of a right-angle prism ($\alpha = 90^{o}$) (a) and a Pythagorian-triangle prism (b) with $\varepsilon = 4$ as a function of the normalized frequency $k_0 a$ and the angle of incidence β, in the H--polariztion case.

C. RCS reduction

In many applications it is desired to reduce RCS that can be done, although only in narrow bands, by selecting specific orientation angle β. A more general approach to the RCS reduction is related to the distortion of the shape of triangle to eliminate the symmetry. It is known that those of the natural modes, which have higher degree of symmetry, display larger values of the corresponding Q-factors.

Indeed, by breaking the symmetry, one can spoil the resonances and make their effect on the RCS values 5-8 times smaller than in the case of an isosceles right-angle prism considered in the previous sub-section (compare panels (a) and (b) in Fig. 5).

IV. ACKNOWLEDGEMENTS

The first author was supported by 2221 Program of the Scientific and Technological Research Council of Turkey (TUBITAK).

REFERENCES

[1] C. Lafargue, M. Lebental, A. Grigis, C. Ulysse, I. Gozhyk, N. Djellali, J. Zyss, and S. Bittner, "Localized lasing modes of triangular organic microlasers," *Phys. Rev. E* 90, 052922, 2014.

[2] H. C. Yin and W. X. Zhang, "EM scattering from a lossy dielectric triangular cylinder based on novel coupled boundary integral equations," *IEEE AP-S Int. Symp.*, pp. 566-569, 1991.

[3] A. F. Peterson, "The 'interior resonance' problem associated with surface integral equations of electromagnetics: numerical consequences and a survey of remedies," *Electromagnetics*, vol. 10, no 3, pp. 293–312, 1990.

[4] D. Wilton, "Review of current status and trends in the use of integral equations in computational electromagnetics," *Electromagnetics*, vol. 12, no 3-4, pp. 287–341, 1992.

[5] C. Muller, Foundations of the Mathematical Theory of Electromagnetic Waves, Berlin, Springer, 1969 (German edition, 1957).

[6] E. I. Smotrova, V. Tsvirkun, I. Gozhyk, C. Lafargue, C. Ulysse, M. Lebental, and A. I. Nosich, "Spectra, thresholds and modal fields of a kite-shaped microcavity laser," *J. Optical Society America B*, vol. 40, no 6, pp. 1732-1742, 2013.

[7] S.V. Boriskina, T.M. Benson, P. Sewell, and A.I. Nosich, "Spectral shift and Q-change of circular and square-shaped optical microcavity modes due to periodic sidewall surface roughness," *J. Opt. Soc. Am. B*, vol. 21, no 10, pp. 1792-1796, 2004.

[8] I. O. Sukharevsky, O. V. Shapoval, A. I. Nosich, and A. Altintas, "Validity and limitations of the median-line integral equation technique in the scattering by material strips of sub-wavelength thickness," *IEEE Trans. Antennas Propag.*, vol. 62, no 7, pp. 3623-3631, 2014.

[9] C. Cugiani, R. Orta, P. Savi, and R. Tascone, "Full-wave investigation of a corner reflector proposed as reference line target for automotive applications," *IEEE Trans. Antennas Propag.*, vol. 45, no 12, pp. 1823-1829, 1997.

[10] N.M. Gunter, Potential Theory and Its Applications to Basic Problems of Mathematical Physics, Frederick Ungar, New York, 1967.